# Dislocations Stabilized by Point Defects Increase Brittleness in PbTe

*James P. Male, Lamya Abdellaoui, Yuan Yu, Siyuan Zhang, Naomi Pieczulewski, Oana Cojocaru-Mirédin, Christina Scheu, and Gerald Jeffrey Snyder\**

Dislocations and the residual strain they produce are instrumental for the high thermoelectric figure of merit, $zT \approx 2$, in lead chalcogenides. However, these materials tend to be brittle, barring them from practical green energy and deep space applications. Nonetheless, the bulk of thermoelectrics research focuses on increasing $zT$ without considering mechanical performance. Optimized thermoelectric materials always involve high point defect concentrations for doping and solid solution alloying. Brittle materials show limited plasticity (dislocation motion), yet clear links between crystallographic defects and embrittlement are hitherto unestablished in PbTe. This study identifies connections between dislocations, point defects, and the brittleness (correlated with Vickers hardness) in single crystal and polycrystalline PbTe with various n- and p-type dopants. Speed of sound measurements show a lack of electronic bond stiffening in p-type PbTe, contrary to the previous speculation. Instead, varied routes of point defect–dislocation interaction restrict dislocation motion and drive embrittlement: dopants with low doping efficiency cause high defect concentrations, interstitial n-type dopants (Ag and Cu) create highly strained obstacles to dislocation motion, and highly mobile dopants can distribute inhomogeneously or segregate to dislocations. These results illustrate the consequences of excessive defect engineering and the necessity to consider both mechanical and thermoelectric performance when researching thermoelectric materials for practical applications.

## 1. Introduction

Practical design problems hinder economically viable heat-to-electricity conversion efficiencies in thermoelectric

generators. Chief among them is the development of compatible n- and p-type thermoelectric materials each with materials figure of merit, $zT$, near 2 across similar temperature ranges. A seemingly obvious candidate, PbTe, can reach $zT$ well above 1 with relative ease for both n- and p-type materials[1,2] at mid-grade waste heat temperatures (similar to Rankine coal cycle temperatures[3]). However, despite continued development since the early 20th century,[4] PbTe materials are rare in modern thermoelectric devices.

High brittleness and sublimation rates in p-type PbTe, but not in n-type, have historically restricted its widespread use.[5–8] NASA's Multi-Mission Radioisotope Thermoelectric Generator (MMRTG) successfully powering the Curiosity and Perseverance rovers employs iodine-doped PbTe for its n-type thermoelectric leg, and a combination of $(Pb,Sn)Te$ and $(AgSbTe_2)_{1-x}(GeTe)_x$ (TAGS) alloys for the p-type leg.[9] The few commercially available, modern PbTe-based devices similarly use low $zT$, Sn alloyed p-type PbTe materials formulated for NASA in the 1960s.[10] Substituting TAGS and $(Pb,Sn)Te$ by even simple, optimally Na-doped p-type PbTe could raise the p-leg $zT$ by a factor of 2 or more (**Figure 1**), but the material's sublimation rates and brittleness may prove to be too restrictive without modifications.

High mechanical hardness is often interpreted as beneficial in PbTe,[15,16–20] which may be misleading in some cases. While strong structural materials are often hard, the advantages/disadvantages of increasing hardness within a system can vary. For example, increasing hardness in dental enamel replacements can help with abrasion resistance,[21] while lowering hardness in brittle martensitic steel increases toughness for structural purposes.[22] Brittle materials like PbTe are limited by their inability to sustain high degrees of plastic deformation. While not a perfect measurement of plasticity, hardness tends to increase when plastic deformation is limited. Thus, a higher hardness (and yield strength) is most likely *detrimental* for PbTe mechanically, unless it is accompanied by increased fracture toughness (resistance to fracture in a cracked material) through strategies like compositing or nanostructuring.[19,23] A link between hardness and brittleness is directly measured in compressive

J. P. Male, N. Pieczulewski, G. J. Snyder
Department of Materials Science and Engineering
Northwestern University
Evanston, IL, USA
E-mail: jeff.snyder@northwestern.edu
L. Abdellaoui, S. Zhang, C. Scheu
Max-Planck-Institut für Eisenforschung GmbH
40237 Düsseldorf, Germany
Y. Yu, O. Cojocaru-Mirédin
Institute of Physics IA
RWTH Aachen University
52056 Aachen, Germany

**ADVANCED
SCIENCE NEWS**
www.advancedsciencenews.com

**ADVANCED
FUNCTIONAL
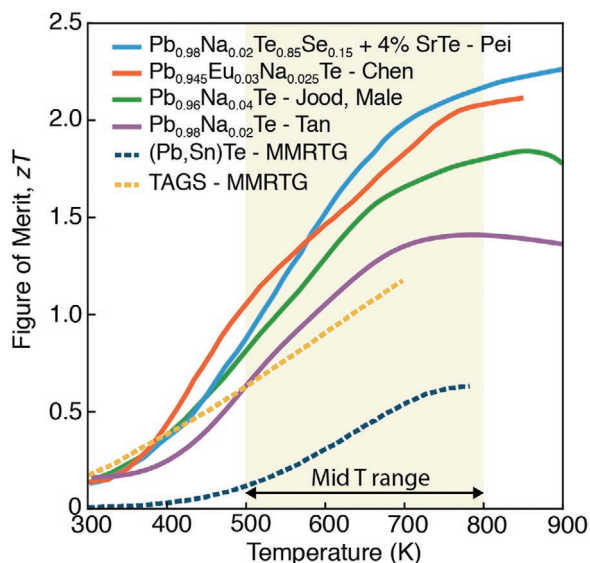MATERIALS**
www.afm-journal.de

**Figure 1.** Some of the highest reported figure of merit ($zT$) p-type PbTe thermoelectric materials compared to the current p-type NASA MMRTG materials.[9,11–14] p-type PbTe's $zT$ is significantly higher than TAGS and PbSnTe across the relevant mid temperature range ($\approx$500–800 K).[9]

experiments in which harder PbTe has a higher yield strength but lower fracture strain. These studies show that PbTe samples with low hardness can handle vastly more plastic deformation before fracture and are therefore mechanically superior to high hardness samples when brittleness is a concern.[5,7]

Recent advances in Pb chalcogenides focus on defect engineering for improved thermoelectric performance with little consideration of coincident effects on mechanical properties.[12,24–27] Introducing high dislocation densities leads to enhanced phonon scattering, increased internal strain, and lattice softening, each of which can lower thermal conductivity and raise $zT$.[17,24,28] As such, researchers subject materials to a battery of plastic deformation, alloying, and disordering to increase dislocation concentrations. In many cases, interactions between dopant elements and dislocations are directly identified using microscopy, signifying a mechanism by which dislocation mobility is limited and internal strain is increased.[29–32] Given that plastic deformation in a crystal relies on dislocations traveling through its lattice, such defect engineering strategies should have obvious and significant effects on brittleness. Indeed, Pb chalcogenides with extensive defect engineering are often measured to have high hardness—an indicator of embrittlement.[17,18,33] If such high performing thermoelectrics are ever to be reliable in real-world use, the effects of defect engineering on mechanical properties must be understood and addressed.

Fundamental studies on mechanical properties in PbTe have found distinct, intriguing contrast between n- and p-type doped samples. For previously studied dopants, hardness appears to be several times higher (and fracture strain several times lower) in heavily doped p-type samples relative to undoped PbTe and n-type PbTe.[5–8] Common explanations for p-type PbTe embrittlement include (1) stiffening from PbTe's heavy $\Sigma$ valence band, and (2) solid solution strengthening by p-type dopant substitution.[5,6] The reasoning behind each is as follows:

1. A heavy mass $\Sigma$ band lies $\approx$ 0.2 eV (at 300 K) below the lighter L point valence band maximum in PbTe. High hole carrier concentrations and/or elevated temperatures increase the $\Sigma$ band's contribution to electronic transport—increasing the density of states effective mass and valley degeneracy.[2,34,35] Previous authors noted that hardness and hole effective mass both increased at the same carrier concentrations in Na-doped p-type PbTe and speculated that $\Sigma$ band contributions may stiffen bonds.[5,7,8]

2. Adding dopants with large ionic size mismatch from their host sites creates local strain. The strain field may interact strongly with dislocations, raising the stress needed to break dislocations free (yield). This phenomenon, "solid solution strengthening," can strengthen steels and structural materials[36] by increasing yield strength, reducing dislocation mobility, and limiting ductility. It follows that greater chemical dissimilarity and ionic size mismatch from the typical p-type doping of Na on the Pb site ($Na'_{Pb}$) might harden more than n-type doping of iodine on Te ($I^{\bullet}_{Te}$).[6,37]

The only past success in reducing PbTe's brittleness followed (1) by exploring the fully miscible PbTe-SnTe system. Heavy alloying with Sn (which increases p-type carrier concentration) hardens PbTe less than Na doping, which may explain why more ductile (Pb,Sn)Te alloys are used in place of higher $zT$ Na-doped PbTe in modern devices.[6–9] In another work, doping p-type with Na while alloying with Cd increased hardness more than Na doping alone.[6] Both results seem to fortify explanation (1) above, as adding Sn to PbTe increases the L-$\Sigma$ gap and reduces $\Sigma$ contributions to transport while Cd does the opposite.[38,39] However, the defects and strain inserted from the chosen additions must be considered. Alloying PbTe with Sn forms a large number of p-type cation vacancies, and Cd is known to increase internal dislocation strain.[33] In this study, we argue that such intrinsic defects and dislocations must become a primary focus when considering PbTe's mechanical properties.

Here, we expand on the role of point defect and dislocation defects in the mechanical properties of PbTe. We explore a wide variety of n- and p-type dopants in both polycrystalline and single crystal PbTe samples and utilize phase boundary mapping techniques[40,41] to exert control over the compensating intrinsic defects that form in response to extrinsic dopants. Classic p-type doping in PbTe creates a large concentration of unfavorable defects due to low doping efficiency, which leads to increased hardness and brittleness. Further, n-type PbTe can be just as hard as p-type PbTe when doped with interstitial dopants like Cu or Ag. PbTe's brittleness appears to result from inhibited plastic behavior from defects rather than electronic band stiffening, and dopant ionic size mismatch is not a sufficient basis for brittleness on its own.

## 2. Results and Discussion

Several hardness tests on n- and p-type PbTe are summarized in **Figure 2**, and will be addressed more specifically in the following sections. See the Supporting Information for full experimental results. Experiments have been guided by phase boundary mapping methods, allowing for precise control of defect type
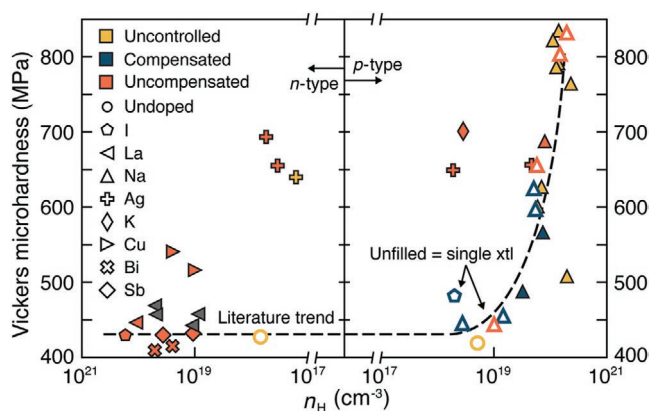
**Figure 2.** Measured Vickers microhardness at different n- and p-type Hall carrier concentrations ($n_H$) for single crystal ((100) face) and polycrystalline PbTe samples with varied dopants of different ionic sizes. Samples that were phase boundary mapped to fix intrinsic defect concentrations are colored blue or orange. "Compensated" samples were synthesized to have a high concentration of compensating defects (minimum extrinsic doping efficiency), and "uncompensated" samples were synthesized to have a low number of compensating defects (maximum doping efficiency). The dashed line shows the PbTe hardness trend observed in previous works.[5–8]

and concentration, as detailed in the Experimental Section. Samples are colored to represent whether they were phase boundary mapped to have high or low doping efficiency, labeled as "uncompensated" and "compensated," respectively. Dopants include La, Na, I, K, Cu, Bi, Sb, and Ag to cover several n- and p-type dopants of different sizes. Additionally, both aligned single crystals (confirmed by Laue back diffraction experiments) and polycrystalline, hot pressed pellets were investigated to remove confounding mechanical effects from grain boundaries. Given the volume and variety of samples synthesized, mechanical tests were limited to relatively simple and fast hardness measurements. However, we note that high hardness samples were markedly more difficult to handle, produced far more brittle cracking during hardness tests, and felt qualitatively more fragile.

## 2.1. No Stiffening from Σ Band Contributions

Measurements described in this section find no Σ band bonding effects substantial enough to cause a massive hardness increase upon p-type doping, as previous works have speculated.[5,7,8] An intuitive proxy for bond stiffness is the speed of sound ($v_s$) through a material. Measured $v_s$ can be directly converted to elastic constant matrices by measuring multiple orientations of single crystals or by making isotropic approximations in polycrystalline samples (see Supporting Information).[42] Simple pulse echo $v_s$ measurements are shown in **Figure 3** for single crystal and polycrystalline samples. If the Σ band were stiffening bonds, one would expect higher $v_s$ at high hole concentrations. In fact, higher Hall carrier concentration ($n_H$) appears to weaken rather than stiffen bonds, perhaps due to electron count softening[43] or higher dislocation density/strain.[24,44] Given that $v_s$ decreases similarly upon n- or p-type doping in Figure 3a (the Σ band only contributes to p-type transport) and that high hardness is observed with certain n-type dopants, it seems the Σ band exclusively
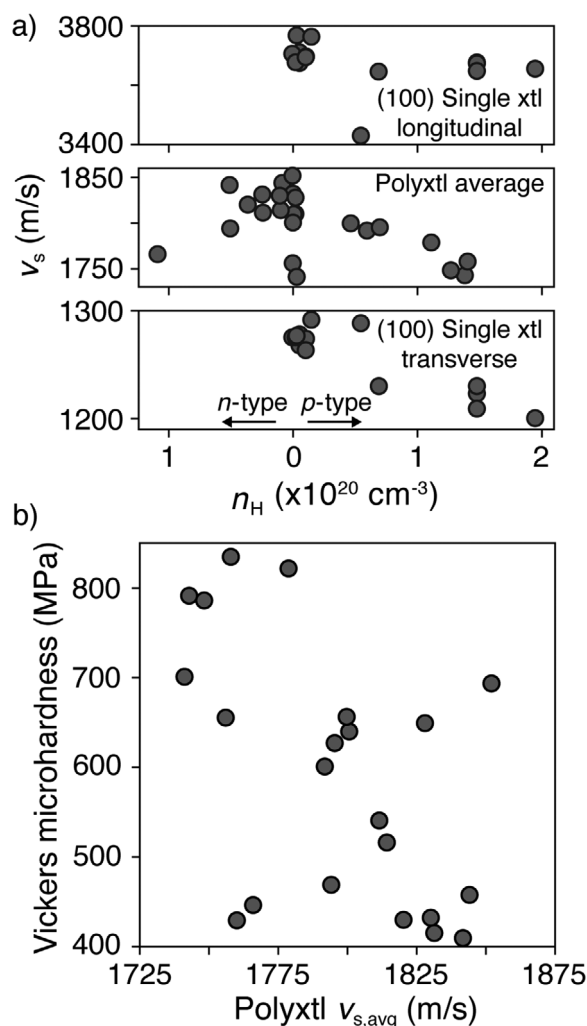


**Figure 3.** a) Speed of sound of n- and p-type PbTe samples with a variety of intrinsic or extrinsic dopants. Top and bottom panels in (a) show longitudinal and transverse wave measurements, respectively, on orientated (100) faces of single crystal samples. The center panel shows measurements on polycrystalline samples, where an average speed of sound is extracted from $v_{avg} = \left( \frac{1}{3} \left[ \frac{1}{v_l^3} + \frac{2}{v_T^3} \right] \right)^{-\frac{1}{3}}$. b) Measured Vickers microhardness showing no strong trend with polycrystalline average speed of sound ($v_{s, avg}$).

influences transport, with no appreciable elastic effects. Correspondingly, there is no clear trend in microhardness with $v_s$ (Figure 3b). Furthermore, the 2× hardness increase in PbTe appears more drastic than that observed in systems where bonds are intentionally stiffened.[45]

Crucially, these findings show that PbTe becomes brittle due to changes in its plasticity (ability to deform without fracture) rather than elasticity (resistance to initial deformation). Indentation hardness measurements, like those performed here, measure plastic deformation from pressing on a material with a fine tip.[46] All else being equal in a hypothetical perfect crystal, a hardness increase might indicate stiffened bonds, which should also be reflected in $v_s$. A real crystal riddled with defects might see an increase in hardness due to defect–dislocation

interactions preventing dislocation movement and plastic deformation. Given the absence of elastic stiffening in Figure 3, the latter explanation—reduced plasticity due to defects—is explored further.

## 2.2. Negligible Hardening from Grain Boundaries

While we did not exhaustively study hardening as a function of grain size, the defining trend in question—a 100% hardness increase above $\approx 10^{19}$ holes/cm$^{-3}$—is clearly independent of the existence of high-angle grain boundaries. Comparing hardness measurements between the polycrystalline samples (grain size $\approx 20 - 150$ µm) and aligned (100) faces of single crystals in Figure 2 shows no significant differences. Thus, the hardening mechanism appears to result from dislocations interacting with defects on a shorter length scale than the grain boundaries in this study, hinting at a crucial role of point defects.

## 2.3. No Dopant Size Mismatch Effect

We performed a simple test of solid solution strengthening as a function of dopant–host ionic size mismatch ($\Delta_{IR}$) by examining a variety of dopants. **Table 1** compares basic hardness trends from Figure 2 to $\Delta_{IR}$ using approximated ionic radii from Shannon.[37] There is no consistent size-dependent strengthening, again indicating that another explanation for hardening is required. Of note is the comparison between n-type doping with Bi or La ($Bi'_{Pb}$ or $La'_{Pb}$) to p-type Na doping ($Na'_{Pb}$). The three dopants, all of which replace a Pb atom, have a near identical $\Delta_{IR}$, yet only $Na^{\bullet}_{Pb}$ increases hardness.

## 2.4. Dislocations Cause Embrittlement

A novel—albeit unsurprising—story explaining brittleness in doped PbTe emerges when considering the outliers in Figure 2. Electronic carriers in PbTe may have relatively negligible effects on mechanical properties based on the lack of bonding effects (Figure 3) and the outlier samples in Figure 2 that defy the pre-

viously established $n_H$ trend. We instead turn to reductions in plasticity due to strong interactions between point defects and dislocations. We note potential strengthening mechanisms in PbTe using observations about doping efficiency (the number of charge carriers added per dopant atom), known strengthening phenomena, and advanced microstructure probes. All explanations offer evidence for a single conclusion that is familiar in basic mechanical properties texts: dense, immobile dislocations lead to embrittlement in PbTe.

High concentrations of point defects like vacancies can lead to embrittlement and increased hardness by collapsing into dislocations and/or hindering dislocation motion.[47] If dopants substitute as shallow defects in PbTe (supported by past works[41,48,49]), a 100 % doping efficiency indicates exactly one charge carrier added per dopant atom and <100 % doping efficiency suggests charge compensation from intrinsic defects with opposite charge to the dopant. General trends in doping efficiency determined in both this study and others[41,50–53] find near $\approx$ 100 % doping efficiency up to high $n_H$ from classic n-type dopants like I and La, while the doping efficiency of p-type dopants drops off steeply at high $n_H$—likely due to pervasive compensating $V^{\bullet\bullet}_{Te}$ and $Te^{\bullet\bullet}_{Pb}$ defects.[14,54–56] Therefore, high p-type $n_H$ values in PbTe require higher (orders of magnitude) concentrations of both doping atoms and intrinsic defects than n-type samples with the same absolute $n_H$. Substitutional p-type Ag and K are less efficient dopants than Na, and likewise have vastly higher intrinsic defect concentrations at low $n_H$. The inherently higher defect concentrations associated with p-type doping relative to n-type doping, as well as lower doping efficiencies in Ag and K dopants may play a key role in explaining high p-type hardness and outlier samples on the p-type side of Figure 2. Other works find low doping efficiency dopants and/or point defects restrict dislocation movement in PbSe[57] and PbS,[58,59] which corroborates the high hardness observed from p-type doping in both systems.[5]

Most samples in this study were phase boundary mapped to lie in Pb- or Te-rich phase equilibria. Pb-rich phase equilibria produces higher doping efficiency for n-type dopants while p-type dopants are more efficient in Te-rich conditions. Samples designated as "uncompensated" in Figure 2 are in a phase equilibrium with maximum doping efficiency, while samples labeled as "compensated" have minimized doping efficiency. Phase equilibrium is unknown in "uncontrolled" samples. Armed with this knowledge, we see a clear example of hardness increasing beyond the expected value due to high intrinsic defect concentrations. Single crystal PbTe doped with iodine, which has a $\approx$ 100% n-type doping efficiency when Pb-rich, shows p-type conduction in Te-rich conditions due to overwhelming $V''_{Pb}$ defects[41] (see the p-type iodine-doped sample in Figure 2). Such high defect concentrations appear to raise hardness in this sample far above any previous observations in iodine-doped PbTe, emphasizing the key hardening role of intrinsic defects.

Differences in compensated versus uncompensated Na-doped PbTe may arise from the different types of intrinsic defects in each. Compensated (Pb-rich) Na-doped samples have primarily $V^{\bullet\bullet}_{Te}$ intrinsic defects, while uncompensated samples have high $Te^{\bullet\bullet}_{Pb}$ concentrations.[14,54–56] Both defects appear to harden PbTe, but generally higher hardness in uncompensated,

**Table 1.** Dopants explored in this study and their relative ionic size differences[37] to their host atoms ($\Delta_{IR}$) shown along with the Vickers microhardness change observed in PbTe doped with the listed dopants relative to undoped PbTe. Samples with "drastic" hardening can show a nearly twofold increase in hardness. Note that interstitial Ag and Cu dopants (the character favored in Pb-rich conditions) are not included here for clarity.

| Dopant | $\Delta_{IR}$ (Å) | Hardening observed |
| --- | --- | --- |
| $I'_{Te}$ | −0.01 | Minimal |
| $La'_{Pb}$ | −0.16 | Minimal |
| $Bi'_{Pb}$ | −0.16 | Minimal |
| $Sb'_{Pb}$ | −0.43 | Minimal |
| $Na^{\bullet}_{Pb}$ | −0.17 | Drastic |
| $K^{\bullet}_{Pb}$ | 0.19 | Drastic |
| $Ag^{\bullet}_{Pb}$ | −0.04 | Drastic |

**ADVANCED
SCIENCE NEWS**
www.advancedsciencenews.com

**ADVANCED
FUNCTIONAL
MATERIALS**
www.afm-journal.de

Na-doped PbTe suggests that $Te^{\bullet\bullet}_{Pb}$ does so more rapidly. The mechanism behind $Te^{\bullet\bullet}_{Pb}$ hardening requires more rigorous examination. However, we note briefly that Pb and Te are not chemically similar and Te may be in an unfavorable and highly strained configuration when losing four electrons to form $Te^{\bullet\bullet}_{Pb}$. Further, a dislocation pinned by a $V''_{Pb}$ defect has a route to "escape," forming a jog from the vacancy when the material yields, while one pinned by a $Te^{\bullet\bullet}_{Pb}$ defect does not. There is precedent for different degrees of strengthening from different intrinsic defects (phase equilibrium) in other well-studied alloys, particularly intermetallics like AgMg,[60,61] although which type of intrinsic defect is more strengthening appears to be system dependent.

Turning to hardness in n-type PbTe, two justifiable outliers arise from Cu or Ag doping. Both elements can be amphoteric (e.g., Ag is a p-type substitutional dopant in Te-rich conditions), but notably dope as n-type interstitials in Pb-rich conditions.[49,57,62] Both elements have lower doping efficiencies than the other n-type dopants studied here and will each be accompanied by high concentrations of p-type $V''_{Pb}$ defects. Ag, which has the lower doping efficiency of the two, may be more hardening than Cu due to its higher $V''_{Pb}$ concentration. Highly strained interstitial defects and high vacancy concentrations can each lead to the unprecedented hardness in these samples,[47,57] and even greater hardening may arise when they are combined in defect complexes. Interstitial defects paired with vacancies create a tetragonal (asymmetric) distortion in rock salt structures like PbTe. Such distortions involve both positive and negative local strain (strain dipole), resulting in a remarkably hard obstacle to dislocation motion[63] and significant hardening.

The dislocation network of Na-doped and I-doped PbTe single crystals were studied using scanning transmission electron microscopy (STEM). **Figure 4**a,b shows STEM low-angle annular dark field (LAADF) micrographs of Te-rich and Pb-rich $Pb_{0.99}Na_{0.01}Te$ samples. The Te-rich analogue contains far more dislocations ($2 \times 10^{10}$ cm$^{-2}$), despite minimal stoichiometric deviation from the Pb-rich sample ($7 \times 10^9$ cm$^{-2}$ dislocations). The parallel dislocation network and the high dislocation density ($> 10^{10}$ cm$^{-2}$) in the single crystal samples in Figure 4a mirror those in highly strained, polycrystalline Eu/Na co-doped PbTe.[32] The Pb-rich, I-doped single crystal presented with a high-angle annular dark field (HAADF)-STEM micrograph in Figure 4c has a similar dislocation density ($6 \times 10^9$ cm$^{-2}$) to the Pb-rich, Na-doped sample. This implies that Na-doped PbTe in Pb-rich conditions may have reduced dislocation density and strain akin to typical n-type dopants. Indeed, when comparing Pb-rich (compensated) to Te-rich (uncompensated) Na-doped samples in Figure 2, Pb-rich samples have markedly lower hardness, perhaps due the aforementioned differences in intrinsic defect character between the two or differences in dopant distributions discussed later.

The discovery in Figure 4 of high dislocation densities from Na doping alone in finely polished single crystals of Te-rich PbTe brings further context to recent work focused on intentionally adding strain and dislocations to Pb chalcogenides. Cd, Cu, Eu, Ga, Ag, and/or Na additions measurably added strain and dislocations to Pb chalcogenides subjected to plastic deformation by ball milling or hot pressing.[12,29–33,44] These dopants enable higher dislocation densities than plastic deformation
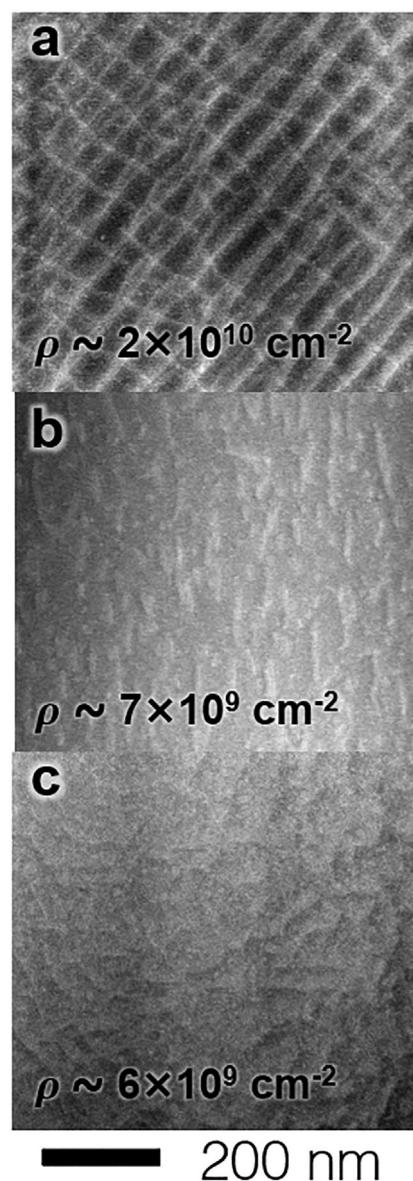


**Figure 4.** STEM images of dislocation networks including STEM-LAADF images of single crystal PbTe doped with nominally 1 at.% Na in a) Te-rich conditions and b) Pb-rich conditions. c) STEM-HAADF image of single crystal Pb-rich PbTe doped with nominally 1 at.% iodine. Dislocation densities (ρ) in each case are annotated onto the image and show far higher concentrations in the Te-rich, Na-doped sample.

alone, as evidenced by an increase in maximum strain from Na/Eu doping in ball milled PbTe.[44] Figure 4 demonstrates that Na has a tendency to increase dislocation density in PbTe without any additional processing. Given our proposed link between dislocations and hardness and the high hardness measured in some highly strained samples,[17,18,33] dopants that tend to add internal strain may also be particularly effective at hardening PbTe. Consequently, hardness measurements appear to be a simple, rough approximation of dislocation density in PbTe.

We utilized atom probe tomography (APT) to verify the proposed defect–dislocation interactions in PbTe. APT measurements in **Figure 5** show greater inhomogeneity in
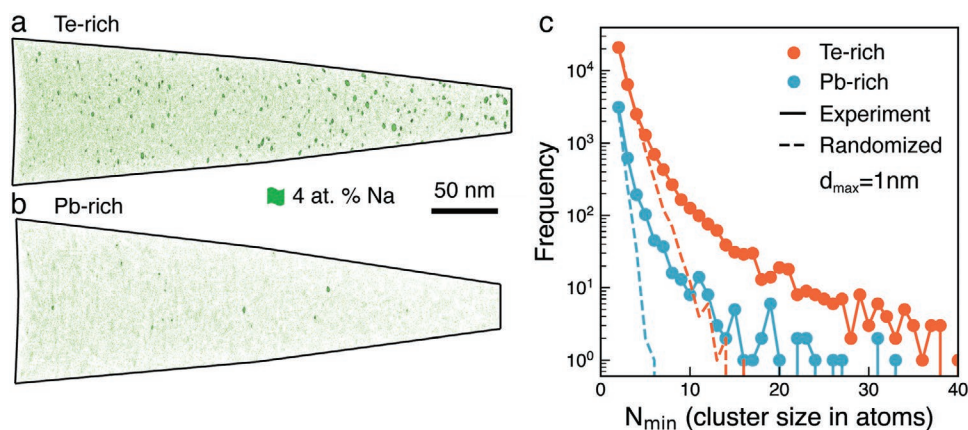
**Figure 5.** Atom probe tomography (APT) measured on single crystals of $Pb_{0.99}Na_{0.01}Te$ prepared in a) Te-rich conditions and b) Pb-rich conditions. Green isosurfaces with $\geq 4.0$ at.% Na have far greater density in the Te-rich tip ($1.1 \times 10^{17}$ cm$^{-3}$) than in the Pb-rich tip ($1.3 \times 10^{16}$ cm$^{-3}$). c) Frequency plots of cluster sizes likewise show higher number densities of Na clusters (determined in a region with maximum diameter of 1 nm as obtained by a nearest neighbor distribution function) in the Te-rich sample ($1.6 \times 10^{17}$ cm$^{-3}$, vs $4.1 \times 10^{16}$ cm$^{-3}$ in the Pb-rich sample). In each sample, Na clustering occurs in greater concentrations than that expected from a randomized distribution of Na atoms.

nominally $Pb_{0.99}Na_{0.01}Te$ single crystals in Te-rich conditions than in Pb-rich conditions. Dopant aggregates (which do not necessarily constitute a secondary phase) appear with a number density of $1.6 \times 10^{17}$ cm$^{-3}$ in the Te-rich sample versus $4.1 \times 10^{16}$ cm$^{-3}$ in the Pb-rich sample. Past works on Pb chalcogenides doped with embrittling Ag, Cu, Na, and/or Eu dopants find similar dopant aggregation[29–32,64] and similar features are responsible for age hardening in structural Al-based and reactor alloys.[65,66] While APT can not identify the non-hardening n-type dopant iodine (I and Te are indiscernible in APT), Bi and La appear to distribute homogenously in PbTe.[67] These observations can be attributed to dopant kinetics. Amphoteric Ag and Cu ions in PbTe can diffuse rapidly through both interstitial sites and vacancies.[68] Na (and similarly, K) dopants are less amphoteric, but still diffuse more rapidly in PbTe than n-type dopants like I or Sb,[51,69] perhaps due to high ionicity and low polarizability in the alkali metals. In the Pb-rich tip (Figure 5b), fewer $V''_{Pb}$ defects relative to Te-rich conditions may explain lower aggregation of Na, which likely diffuses primarily along cation vacancies. Dopant inhomogeneities can pin dislocations and increase hardness, and in some instances the mobile dopants may decorate dislocations, freezing them in the lattice.

### 2.5. Application to Thermoelectric Performance

Modern breakthroughs in PbTe and other Pb chalcogenides specifically introduce large concentrations of point defects and dislocations in pursuit of lowered thermal conductivity and band engineering.[12,17,24,33,47] Dislocations, in particular, can reduce thermal conductivity through lattice softening and phonon scattering[24,32] with minimal reductions in electronic mobility above room temperature.[47,70] Unfortunately, because brittleness and hardening in PbTe embody the resistance to dislocation movement, the same defect engineering strategies may compromise mechanical performance. However, it is still crucial to push the boundaries of $zT$. Assuming brittleness may be associated with some benefits to thermoelectric performance,

the mechanisms identified to increase hardness in this work may therefore serve as useful for improving thermoelectric performance. Notably, we find that most p-type dopants appear effective for adding dislocations to PbTe due to their defect energetics and doping efficiencies—even in single crystal samples that are not subjected to plastic deformation during synthesis (i.e., hot pressing or ball milling). This may contribute to the generally higher $zT$ values in p-type PbTe relative to n-type, despite fairly low doping efficiencies in the known p-type dopants. Choosing mobile dopants that are likely to interact with dislocations may also increase dislocation densities. Interstitial n-type dopants, like Ag and Cu, are particularly useful for adding dislocations and may be a promising route towards competitive $zT$ values in n-type PbTe. Indeed, recent reports of impressive performance in n-type Pb chalcogenides use such dopants to engineer dislocations.[12,29]

We note some promising routes toward suppressing brittleness while maintaining the high thermoelectric performance enabled by defect engineering in PbTe. High strain and dislocation density in PbTe can persist at high temperatures in pressed pellets.[17,26] However, exposing the precursor powder to high temperatures rapidly and drastically reduces strain, indicating a quick and easy method to remove dislocations without affecting dopant additions.[44] We also find consistently lower hardness in p-type Na-doped samples in Pb-rich conditions than Te-rich conditions in this study. While Pb-rich phase equilibrium is inferior for thermoelectric performance, $zT$ in Pb-rich, Na-doped samples may still be adequate if one seeks improved mechanical performance.[14,50] Finally, strategies like making nanocomposites[71] can increase fracture toughness without drastically reducing thermoelectric performance and may be a remedy to restrictively high brittleness.[23,72]

### 3. Conclusions

The mechanical properties of PbTe-based thermoelectric materials have been historically misunderstood. We find brittleness

correlated with dislocation density, as commonly seen in metals. Because dislocations are also known to improve $zT$, a new trade-off is identified when introducing dislocations between improving $zT$ and the additional brittleness that may prevent the material's use in power generation applications. In the process we find Vickers hardness an easy to measure indicator of dislocation density. Overlooking the connection between brittleness and high $zT$ via dislocation density has made meaningful work towards synthesizing less brittle PbTe scant or misdirected. PbTe was previously observed to be brittle only when p-type, suggesting that electronic carriers may play a large role in embrittlement. By studying hardening from a wide variety of n- and p-type dopants, we find scarce effects of electronic carriers on bonding. Rather, PbTe's mechanical properties are better understood by considering classic defect strengthening mechanisms. High point defect concentrations, point defect clustering, and highly strained point defect configurations can hinder dislocation motion and increase hardness, thus making brittle materials more brittle. In PbTe, each of these situations may be driving factors leading to embrittlement. Pervasively lower p-type doping efficiency in PbTe leads to vastly higher concentrations of point defects from both dopant atoms and intrinsic defects relative to classic n-type doping, which may lead to dislocation pinning and formation. Dopants that embrittle PbTe also tend to diffuse easily in the lattice leading to dopant cluster formation observed in this study and others. Cu and Ag dopants in Pb-rich PbTe provide a unique example of brittleness in n-type PbTe, which may stem from a combination of low doping efficiency, high diffusivity, and highly strained defect environments in the n-type interstitial configuration. Understanding the exact extent to which each of these mechanisms contributes to hardening will require multiple meticulous studies and additional contributions may be explored, such as the role of dislocation charge. Regardless, this work provides a new perspective on mechanical properties in PbTe and uncovers the key role of dislocations and point defects in embrittlement. If PbTe-based thermoelectric materials are to be used for green power generation going forward, a balance must be struck between the benefits to thermoelectric performance and the detrimental mechanical consequences of extensive defect engineering.

## 4. Experimental Section

*Sample Synthesis*: PbTe samples were synthesized with different stoichiometries depending on the choice of dopants. For dopants (D) substituting on the Pb site (D = Na, K, Ag, Bi, Sb, La), samples followed the stoichiometry $Pb_{1-x}D_xTe$. Interstitial dopants (Cu, Ag) were added with stoichiometry $PbD_xTe$ and Te substitutions (I) led to $PbTe_{1-x}D_x$. Full stoichiometries are given in the Supporting Information. The oxidized surfaces of the bulk Na and K and the Pb rod were scraped away before use, and elemental La was arc melted for purification. Otherwise, the remaining elements were used as-is (99.99+% pure, metals basis—Alfa Aeasar, USA).

Samples were loaded into carbon-coated quartz ampoules in an Ar-filled glovebox, evacuated to high vacuum, flame sealed, and melted in tube furnaces above 1273 K for at least 2 h. For polycrystalline synthesis, tubes were air quenched through solidification, then dropped into water. The resulting ingots were hand ground and sieved to produce powder size between 20–150 μm and densified by hot pressing at 773 K under 45 MPa for 20 min in an induction hot press. The resulting pellets were > 95% dense, with the majority > 98% by Archimedes density

measurements. Single crystal growth from the melt was achieved by slow cooling to 1122 K at a rate of 0.5 K h$^{-1}$, then dropping to room temperature in the furnace at an uncontrolled rate. The resulting single crystals were visibly inspected, aligned using a flashlight to search for reflections, then sliced using a diamond wire saw. Orientations were quantified using Laue back reflection, which revealed the (100) faces studied here were within 3 degrees of the target orientation.

Approximately 0.5 at % excess Pb or Te was added in most polycrystalline samples while weighting elements following the phase boundary methodology.[73] This allowed for precise control over the type of defects forming in the lattice. Excess elemental Te or Pb additions placed the samples in Te- or Pb-rich phase equilibrium, respectively and changed defect formation energy as a result. For example, $V''_{Pb}$ defects form more readily in Te-rich phase equilibrium than Pb-rich equilibrium. Single crystal samples were phase boundary mapped using a saturation annealing technique to avoid impurity phases.[41] In this process, samples were sealed in an evacuated quartz ampoule along with some sacrificial PbTe saturating media. The saturating media was made using a basic melt–quench technique and doped to the same level as the single crystal samples but with an extra 1 at.% of Pb or Te. The ampoules, each containing both a single crystal and saturating media, were annealed in a furnace at 773 K for 5 days, then quenched in ice water. During annealing, vapor mediates equilibrium between the single crystal sample and the elemental Pb or Te in the saturating media, fixing single crystal sample to Pb or Te-rich equilibrium without physically adding impurities to the sample. A number of samples were not phase boundary mapped, and are denoted as "uncontrolled" in Figure 2.

*Property Measurements*: Vickers microhardness measurements were performed using a Struers Duramin 5. Each PbTe sample was polished in incremental steps up to a 1 μm diamond paste finish while maintaining minimal thickness deviation. Polished sample faces were indented with loads of of 10, 50, and/or 100 g, each for 5 s. The relative trends in hardness were unaffected by the chosen load, and the 50 g load hardness values are reported in this work. Each load was applied several times at varied locations in the sample, all at least three indentation widths away from edges, large scratches, or other indentation marks. In single crystalline samples, only hardness measured on the (100) face is reported. Deviation in hardness values was consistently < 5% for a given load. Indentations were visibly different in low hardness samples versus those with high hardness. Lower hardness samples frequently indented with no surrounding cracks, while spalling and widespread, brittle cracking were observed around the indents in high hardness samples.

Speed of sound measurements were taken using a pulse echo speed of sound system with 5 MHz transducers. The system in question is expected to have 0.6% deviation for a perfectly flat sample, based on standard YAG measurements.[24] Transducers producing either longitudinal or transverse sound waves were affixed to flat, finely polished samples using honey as a coupling agent. Sound wave reflections were observed with a digital oscilloscope. The reflection peaks were corrected for cross-correlations and the time interval between them was used along with sample thickness to determine sound velocity. In polycrystalline PbTe samples, an average sound velocity ($v_s$) was calculated using the longitudinal ($v_L$) and transverse ($v_T$) sound wave velocities through $v_s = (1/3[1/v_L^3 + 2/v_T^3])^{-1/3}$ assuming crystal isotropy.[42] In single crystal samples, where the isotropic approximation is no longer valid, we report $v_L$ and $v_T$ from only the (100) face of single crystals in Figure 3. Additional single crystal orientations are described in the Supporting Information.

Room temperature Hall carrier concentration was measured using a home built Van Der Pauw setup. Measurements were made using pressure-assisted Mo contacts in a 2 T magnetic field from a water cooled electromagnet.

*Microstructure Characterization*: STEM on Na- and I-doped samples was performed using a Titan Themis microscope with an aberration-corrected probe (size of ≈1 Å and convergence semi-angle of 24 mrad) operated at 300 kV. LAADF and HAADF images were set up with collection semi-angle ranges of 17–73 and 73–200 mrads, respectively. The STEM sample was prepared using a dual beam focused ion beam

**ADVANCED**
**SCIENCE NEWS**

www.advancedsciencenews.com

**ADVANCED**
**FUNCTIONAL**
**MATERIALS**

www.afm-journal.de

(FIB)/scanning electron microscope (SEM) (Scios2, Thermo Fisher Scientific).

Dislocation density was estimated from the total length of dislocation lines in STEM micrographs (Figure 4) over the imaging volume, according to $\rho_{dis} = \Sigma l/A/H$ with $l$ being the length of the dislocation line, $H$ the sample thickness measured from FIB, and $A$ the area of STEM images.

Needle-shaped APT specimens were prepared using a dual beam SEM/FIB instrument (Helios NanoLab650, Thermo Fisher Scientific) following the standard "lift-out" method. APT measurements were performed on a local electrode atom probe (LEAP$^{TM}$ 4000X Si, CAMECA) by applying 10 ps, 20 pJ ultraviolet (wavelength = 355 nm) laser pulses with a detection rate of 1 ion per 100 pulses on average, a pulse repetition rate of 200 kHz at a base temperature of 40 K, and an ion flight path of 160 mm. The detection efficiency is limited to 50 % due to the open area left between the microchannels on the detector plates. The data reconstruction and analysis were processed using the IVAS$^{TM}$ 3.8.0.

## Supporting Information

Supporting Information is available from the Wiley Online Library or from the author.

## Acknowledgements

## Conflict of Interest

The authors declare no conflict of interest.

## Data Availability Statement

The data that support the findings of this study are available from the corresponding author upon reasonable request.

## Keywords

[1] G. Tan, M. G. Kanatzidis, in *Materials Aspect of Thermoelectricity* (Ed: C. Uher), CRC Press, Boca Raton **2016**, pp. 125–157, Ch. 4.

[2] A. D. Lalonde, Y. Pei, H. Wang, G. Jeffrey Snyder, *Mater. Today* **2011**, *14*, 526.

[3] C. B. Vining, *Nat. Mater.* **2009**, *8*, 83

[4] M. V. Vedernikov, E. K. Iordanishvili, in *17th International Conf. on Thermoelectrics. Proc. ICT98* **1998**, pp. 37–42.

[5] M. S. Abvola, *Sov. Phys. - Solid State.* **1971**, *12*, 2910.

[6] A. J. Crocker, M. Wilson, *J. Mater. Sci.* **1978**, *13*, 833.

[7] Y. Gelbstein, G. Gotesman, Y. Lishzinker, Z. Dashevsky, M. P. Dariel, *Scr. Mater.* **2008**, *58*, 251.

[8] Y. Gelbstein, Z. Dashevsky, M. P. Dariel, *J. Appl. Phys.* **2008**, *104*, 33702.

[9] J. F. Zakrajsek, D. F. Woerner, J.-P. Fleurial, NASA Special Session: Next-Generation Radioisotop Thermoelectric Generator (RTG) Discussion **2017**, https://rps.nasa.gov/resources/69/next-generation-radioisotope-thermoelectricgenerator-presentation.

[10] P. Bertreau, Ph.D. thesis, Massachusetts Institute of Technology **2006**.

[11] G. Tan, F. Shi, S. Hao, L.-D. Zhao, H. Chi, X. Zhang, C. Uher, C. Wolverton, V. P. Dravid, M. G. Kanatzidis, *Nat. Commun.* **2016**, *7*, 12167.

[12] Z. Chen, Z. Jian, W. Li, Y. Chang, B. Ge, R. Hanus, J. Yang, Y. Chen, M. Huang, G. J. Snyder, Y. Pei, *Adv. Mater.* **2017**, *29*, 1606768.

[13] Y. Pei, G. Tan, D. Feng, L. Zheng, Q. Tan, X. Xie, S. Gong, Y. Chen, J. F. Li, J. He, M. G. Kanatzidis, L. D. Zhao, *Adv. Energy Mater.* **2017**, *7*, 1601450.

[14] P. Jood, J. Male, S. Anand, Y. Matsushita, Y. Takagiwa, M. G. Kanatzidis, G. J. Snyder, M. Ohta, *J. Am. Chem. Soc.* **2020**, *142*, 15464.

[15] C. Gayner, N. Nandihalli, *Materialia* **2020**, *14*, 100912.

[16] S. Sarkar, X. Zhang, S. Hao, X. Hua, T. P. Bailey, C. Uher, C. Wolverton, V. P. Dravid, M. G. Kanatzidis, *ACS Energy Lett.* **2018**, *3*, 2593.

[17] Y. Wu, Z. Chen, P. Nan, F. Xiong, S. Lin, X. Zhang, Y. Chen, L. Chen, B. Ge, Y. Pei, *Joule* **2019**, *3*, 1276.

[18] J. Zhou, Y. Wu, Z. Chen, P. Nan, B. Ge, W. Li, Y. Pei, *Small Struct.* **2021**, 2100016.

[19] J. E. Ni, E. D. Case, K. N. Khabir, R. C. Stewart, C.-I. Wu, T. P. Hogan, E. J. Timm, S. N. Girard, M. G. Kanatzidis, *J. Mater. Sci. Eng. B* **2010**, *170*, 58.

[20] M. H. Lee, S. Park, J. K. Lee, J. Chung, B. Ryu, S.-D. Park, J.-S. Rhyee, *J. Mater. Chem. A* **2019**, *7*, 16488.

[21] K. J. Chun, J. Y. Lee, *Journal of Dental Biomechanics* **2014**, *5*, 1.

[22] G. Krauss, *Mater. Sci. Eng., A* **1999**, *273-275*, 40.

[23] G. Li, U. Aydemir, B. Duan, M. T. Agne, H. Wang, M. Wood, Q. Zhang, P. Zhai, W. A. Goddard, G. J. Snyder, *ACS Appl. Mater. Interfaces* **2017**, *9*, 40488.

[24] R. Hanus, M. T. Agne, A. J. Rettie, Z. Chen, G. Tan, D. Y. Chung, M. G. Kanatzidis, Y. Pei, P. W. Voorhees, G. J. Snyder, *Adv. Mater.* **2019**, *31*, 1900108.

[25] G. Tan, S. Hao, R. C. Hanus, X. Zhang, S. Anand, T. P. Bailey, A. J. E. Rettie, X. Su, C. Uher, V. P. Dravid, G. J. Snyder, C. Wolverton, M. G. Kanatzidis, *ACS Energy Lett.* **2018**, *3*, 705.

[26] Y. Wu, P. Nan, Z. Chen, Z. Zeng, S. Lin, X. Zhang, H. Dong, Z. Chen, H. Gu, W. Li, Y. Chen, B. Ge, Y. Pei, *Research* **2020**, *2020*, 1.

[27] M. H. Lee, J. H. Park, S. D. Park, J. S. Rhyee, M. W. Oh, *J. Alloys Compd.* **2019**, *786*, 515.

[28] T. J. Slade, S. Anand, M. Wood, J. P. Male, K. Imasato, D. Cheikh, M. M. Al Malki, M. T. Agne, K. Griffith, S. K. Bux, C. Wolverton, M. G. Kanatzidis, J. G. Snyder, *Joule* **2021**, *5*, 1168.

[29] Y. Yu, S. Zhang, A. M. Mio, B. Gault, A. Sheskin, C. Scheu, D. Raabe, F. Zu, M. Wuttig, Y. Amouyal, O. Cojocaru-Mirédin, *ACS Appl. Mater. Interfaces* **2018**, *10*, 3609.

[30] C. Zhou, Y. Yu, Y. L. Lee, B. Ge, W. Lu, O. Cojocaru-Mirédin, J. Im, S. P. Cho, M. Wuttig, Z. Shi, I. Chung, *J. Am. Chem. Soc.* **2020**, *142*, 15172.

[31] P. Y. Deng, K. K. Wang, J. Y. Du, H. J. Wu, *Adv. Funct. Mater.* **2020**, *30*, 2005479.

[32] L. Abdellaoui, Z. Chen, Y. Yu, T. Luo, R. Hanus, T. Schwarz, R. Bueno Villoro, O. Cojocaru-Mirédin, G. J. Snyder, D. Raabe, Y. Pei, C. Scheu, S. Zhang, *Adv. Funct. Mater.* **2021**, *31*, 2101214.

[33] Y. Wu, P. Nan, Z. Chen, Z. Zeng, R. Liu, H. Dong, L. Xie, Y. Xiao, Z. Chen, H. Gu, W. Li, Y. Chen, B. Ge, Y. Pei, *Adv. Sci.* **2020**, *7*, 12.

[34] H. Sitter, K. Lischka, H. Heinrich, *Phys. Rev. B* **1977**, *16*, 680.

[35] R. S. Allgaier, *J. Appl. Phys.* **1961**, *32*, 2185.

[36] T. H. Courtney, *Mechanical Behavior of Materials*, 2nd ed., Waveland Press, Inc., Long Grove **2000**.

[37] R. D. Shannon, *Acta Cryst.* **1976**, *32*, 751.

[38] E. M. Hedegaard, A. A. Mamakhel, H. Reardon, B. B. Iversen, *Chem. Mater.* **2018**, *30*, 280.

[39] K. Ahn, K. Biswas, J. He, I. Chung, V. Dravid, M. G. Kanatzidis, *Energy Environ. Sci.* **2013**, *6*, 1529.

[40] S. Ohno, U. Aydemir, M. Amsler, J. H. Pöhls, S. Chanakian, A. Zevalkink, M. A. White, S. K. Bux, C. Wolverton, G. J. Snyder, *Adv. Funct. Mater.* **2017**, *27*, 1606361.

[41] J. Male, M. T. Agne, A. Goyal, S. Anand, I. T. Witting, V. Stevanović, G. J. Snyder, *Mater. Horiz.* **2019**, *6*, 1444.

[42] O. Anderson, *J. Phys. Chem. Solids* **1963**, *24*, 909.

[43] T. J. Slade, S. Anand, M. Wood, J. P. Male, K. Imasato, D. Cheikh, M. M. Al Malki, M. T. Agne, K. Griffith, S. K. Bux, C. Wolverton, M. G. Kanatzidis, J. G. Snyder, *Joule* **2021**, *5*, 1168.

[44] J. P. Male, R. Hanus, J. G. Snyder, R. P. Hermann, *Chem. Mater.* **2021**, *33*, 4765.

[45] A. Šimůnek, J. Vackář, *Phys. Rev. Lett.* **2006**, *96*, 8.

[46] J. S. Tse, *J. Superhard Mater.* **2010**, *3*, 46.

[47] Z. Chen, B. Ge, W. Li, S. Lin, J. Shen, Y. Chang, R. Hanus, G. J. Snyder, Y. Pei, *Nat. Commun.* **2017**, *8*, 13828.

[48] S. Bajaj, H. Wang, J. W. Doak, C. Wolverton, G. Jeffrey Snyder, *J. Mater. Chem. C* **2016**, *4*, 1769.

[49] B. Ryu, M.-W. Oh, J. K. Lee, J. E. Lee, S.-J. Joo, B.-S. Kim, B.-K. Min, H.-W. Lee, S.-D. Park, *J. Appl. Phys.* **2015**, *118*, 015705.

[50] X. Wang, I. Veremchuk, M. Bobnar, U. Burkhardt, J.-T. Zhao, Y. Grin, *Chem. Mater.* **2018**, *30*, 1362.

[51] Y. Noda, M. Orihashi, I. A. Nishida, *Mater. Trans., JIM* **1998**, *39*, 602.

[52] Q. Zhang, F. Cao, W. Liu, K. Lukas, B. Yu, S. Chen, C. Opeil, D. Broido, G. Chen, Z. Ren, *J. Am. Chem. Soc.* **2012**, *134*, 10031.

[53] Y. Pei, Z. M. Gibbs, A. Gloskovskii, B. Balke, W. G. Zeier, G. J. Snyder, *Adv. Energy Mater.* **2014**, *4*, 1.

[54] J. W. Doak, K. J. Michel, C. Wolverton, *J. Mater. Chem. C* **2015**, *3*, 10630.

[55] A. Goyal, P. Gorai, E. S. Toberer, V. Stevanović, *npj Comput. Mater.* **2017**, *3*, 42.

[56] X. Zhang, M. Y. Toriyama, J. P. Male, Z. Feng, S. Guo, T. Jia, Z. Ti, G. J. Snyder, Y. Zhang, *Mater. Today Phys.* **2021**, *19*, 100415.

[57] J. A. Grovogui, T. J. Slade, S. Hao, C. Wolverton, M. G. Kanatzidis, V. P. Dravid, *J. Mater. Res.* **2021**, 1.

[58] F. C. Frank, in *Discussions of the Faraday Society* **1957**, pp. 122–127.

[59] L. Fu, J. Cui, Y. Yu, Y. Huang, Y. Wang, Y. Chen, J. He, *J. Mater. Chem. A* **2019**, *7*, 6304.

[60] T. Mitchell, in *Encyclopedia of Materials: Science and Technology*, vol. 1, Elsevier, Amsterdam **2001**, pp. 9827–9842.

[61] R. L. Fleischer, D. M. Dimiduk, H. A. Lipsitt, *Annu. Rev. Mater. Sci.* **1989**, *19*, 231.

[62] Y. Xiao, H. Wu, W. Li, M. Yin, Y. Pei, Y. Zhang, L. Fu, Y. Chen, S. J. Pennycook, L. Huang, J. He, L. D. Zhao, *J. Am. Chem. Soc.* **2017**, *139*, 18732.

[63] R. L. Fleischer, *Acta Metall.* **1962**, *10*, 835.

[64] A. Sheskin, T. Schwarz, Y. Yu, S. Zhang, L. Abdellaoui, B. Gault, O. Cojocaru-Mirédin, C. Scheu, D. Raabe, M. Wuttig, Y. Amouyal, *ACS Appl. Mater. Interfaces* **2018**, *10*, 38994.

[65] P. Dumitraschkewitz, S. S. Gerstl, L. T. Stephenson, P. J. Uggowitzer, S. Pogatscher, *Adv. Eng. Mater.* **2018**, *20*, 1800255.

[66] L. Liu, K. Nishida, K. Dohi, A. Nomoto, N. Soneda, K. Murakami, Z. Li, D. Chen, N. Sekimura, *J. Nucl. Sci. Technol.* **2016**, *53*, 1546.

[67] Y. Pei, J. Lensch-Falk, E. S. Toberer, D. L. Medlin, G. J. Snyder, *Adv. Funct. Mater.* **2011**, *21*, 241.

[68] C. C. Li, F. Drymiotis, L. L. Liao, H. T. Hung, J. H. Ke, C. K. Liu, C. R. Kao, G. J. Snyder, *J. Mater. Chem. C* **2015**, *3*, 10590.

[69] R. Dalven, *Infrared Phys.* **1969**, *9*, 141.

[70] R. S. Allgaier, W. W. Scanlon, *Phys. Rev.* **1958**, *111*, 1029.

[71] N. A. Heinz, T. Ikeda, Y. Pei, G. J. Snyder, *Adv. Funct. Mater.* **2014**, *24*, 2135.

[72] G. Cerretti, O. Villalpando, J. P. Fleurial, S. K. Bux, *J. Appl. Phys.* **2019**, *126*, 175102.

[73] S. Ohno, K. Imasato, S. Anand, H. Tamaki, S. D. Kang, P. Gorai, H. K. Sato, E. S. Toberer, T. Kanno, G. J. Snyder, *Joule* **2018**, *2*, 141.